Supplementary information

Covalent organic frameworks with high quantum efficiency in photocatalytic hydrogen evolution: mediating charge separation

Chunzhi Li,[a,c] Jiali Liu,[a,c] He Li,[a,*] Kaifeng Wu,[d] Junhui Wang,[d,*] Qihua Yang[a,b*]

[a] State Key Laboratory of Catalysis, Dalian Institute of Chemical Physics, Chinese Academy of Sciences, 457 Zhongshan Road, Dalian 116023, China.

[b] Key Laboratory of the Ministry of Education for Advanced Catalysis Materials, Zhejiang Key Laboratory for Reactive Chemistry on Solid Surfaces, Institute of Physical Chemistry, Zhejiang Normal University, Jinhua 321004, China.

[c] University of Chinese Academy of Sciences, Beijing 100049, China.

[d] State Key Laboratory of Molecular Reaction Dynamics, Dalian Institute of Chemical Physics, Chinese Academy of Sciences, 457 Zhongshan Road, Dalian 116023, China.

Email addresses: lihe@dicp.ac.cn, wjh@dicp.ac.cn, yangqh@dicp.ac.cn.

Supplementary Methods.

Materials and instrumentation

All chemicals used in this study were of analytical grade and used as received unless otherwise specified.

Thermal gravimetric analyses (TGA) were performed on a NETZSCH STA 449F3 analyzer, with a temperature range from 30 to 100 ^{o}C and a heating rate of 10 ^{o}C min^{-1} in air atmosphere. Powder x-ray powder diffraction (PXRD) patterns were measurement on a Rigaku RINT D/Max-2500 powder diffraction system, equipped with Cu Kα radiation (λ = 1.54 Å). Transmission electron microscopy (TEM) images were collected using a HITACHI HT7700 microscope at an acceleration voltage of 100 kV. High-resolution transmission electron microscopy (HRTEM) analysis was performed using a JEM-2100 microscope. Scanning electron microscopy (SEM) characterizations were collected using JSM-7900F. Atomic force microscopy (AFM) analysis was performed using Nano Wizard Ultra Speed &inVia Raman. Dynamic light scattering (DLS) experiments were performed using Zetasizer Nano. Nitrogen sorption characterization was performed on an automatic volumetric adsorption analyzer (Micromeritics ASAP2020). Before analysis, all the samples were carefully degassed at 100 ^{o}C for 6 hours under the vacuum of 10 mmHg. The BET surface area was calculated from the adsorption data in a relative partial pressure (P/P_0) range of 0.04 to 0.20. The total pore volume was calculated at P/P_0 of 0.99 using a single-point adsorption value. The pore diameter was determined from the adsorption branch by using the Non-Localized Density Functional Theory (NLDFT) method. The Fourier-transform infrared spectroscopy (FT-IR) spectra were recorded from 400-4000 cm^{-1} on a Nicolet Nexus 470 IR spectrometer by using KBr pellets. All samples were dried with an infrared lamp before analysis. Solid-state ^{13}C CP-TOSS NMR spectra were performed on a Bruker 600 MHz spectrometer. ^{13}C and signals were referenced to tetramethylsilane (TMS). UV/Vis absorption spectra were recorded on SHIMADZU UV-Vis 2550 spectrophotometer.

Mott-Schotty plots and measurement was performed using a CH Instruments Model 760E electrochemical work station (CHI760E). The as-prepared materials were dispersed in a mixture of ethanol and Nafion (5 wt% in ethanol) by sonication and then casted onto the pre-treated glassy carbon electrode (GCE) surface. The Mott-Schotty plots measurements were conducted in a three-electrode single cell,

with the COF/GCE as the working electrode, a Pt plate as the counter electrode, and a saturated mercury electrode (SCE) as the reference electrode. The electrolyte was deionized water containing with 0.20 M Na_2SO_4.

Structural modeling of CN-COF

The process of simulating COF structure was performed by the Materials Studio software. The hexagonal lattice with P6/M symmetry group was set as the initial eclipsed COF structure. After the smallest asymmetric fragment was filled into the blank cell, the Forcite tools package was employed to optimize the cell geometry including energy minimization. The AB stacking structure was built with the similar process as described above, with the exception that a supercell with double c value was selected as the initial cell of staggered structure. The cell optimized from the Universal force fields was subsequently refined using the Pawley refinement method in Reflex tools.

Computational method of charge distribution

We have employed the VASP[1,2] to perform all the spin-polarized density functional theory (DFT) calculations within the generalized gradient approximation (GGA) using the Perdew-Burke-Ernzerhof (PBE)[3] formulation. We have chosen the projected augmented wave (PAW) potentials[4] to describe the ionic cores. Take valence electrons into account using a plane wave basis set with a kinetic energy cutoff of 450 eV. Partial occupancies of the Kohn−Sham orbitals were allowed using the Gaussian smearing method and a width of 0.05 eV. The electronic energy was considered self-consistent when the energy change was smaller than 10−5 eV. A geometry optimization was considered convergent when the energy change was smaller than 0.03 eV/Å. The brillouin zone is sampled with 1 × 1 × 1 Gamma mesh[5].

AQE measurement

The AQE was measured using a 300 W Xe lamp (PLS-FX300, Perfectlight) with different band-pass filters of 400, 450, 500, 550, 600 and 650 nm. The number of incident photons reaching the solution was measured using a calibrated Si photodiode (LS-100, EKO Instruments Co., LTD). The numbers of photons were counted according to a litrature method[6] using photon-to-current conversion with a Si photodiode and a multimeter in the device shown in Supplementary Figure 20. The AQE was calculated using the following equation:

$$\mathrm{AQE} = \frac{2 \times number\ of\ evolved\ H_2\ molecules}{number\ of\ incident\ photons} \times 100\%$$

The numbers of photons were measured at various positions by sliding the position of a Si photodiode with an interval of 3 mm, the total incident photons can be then calculated by numerically integrating the obtained data over the entire light acceptance area (7.5 cm ×7.5 cm) of the reactor.[6] The total numbers of incident photons at the wavelength of 400, 450, 500, 550 600 and 650 nm were summarized in Supplementary Figure 20.

Photocatalytic hydrogen evolution with thin CN-CON film

The thin CN-CON film deposited on glass support was prepared as follows. 2 mg of CN-CON powder (deposited with 1 wt% Pt) and 200 μL Nafion (5 wt% in ethanol) were added into ethanol (1 mL), and the mixture was sonicated for 1 h. After sonication, a colloidal solution was formed. Thin CN-CON film was prepared by drop-casting the solution onto roughened glass. The resulting film was dried at 120 ^{o}C for 6 h. For the hydrogen evolution experiment using CN-CON film, the CN-CON coated glass was immersed in a flask with quartz filter containing 0.1 M ascorbic acid water solution (100 mL). The resulting mixture was degassed by Ar bubbling for 30 minutes. The reaction system was irradiated with a 300 W Xe lamp (PLS-FX300, Perfectlight) for the time specified using cut-on filters ($\lambda > 420$ nm) without stirring. Gas samples were taken with a gas-tight syringe (Hamilton 1700) and the HER rate was analyzed by GC.

Photocatalytic oxygen evolution

A flask with quartz filter was charged with CN-CON (20 mg), a certain amount of $Co(NO_3)_2$ as a co-catalyst, 100 mL water containing 5 mmol $AgNO_3$, and 100 mg of La_2O_3 as pH buffer agent. The resulting mixture was sonicated for 10 minutes before degassing by Ar bubbling for 30 minutes. The reaction system was irradiated with a 300 W Xe lamp (PLS-FX300, Perfectlight) for the time specified using cut-on filters ($\lambda > 420$ nm). Gas samples were taken with a gas-tight syringe (Hamilton 1700) and run on a gas chromatograph (Agilent 8860) equipped with Molecular Sieve 5A column connected to thermal conductivity detector.

Supplementary Figures and Tables.

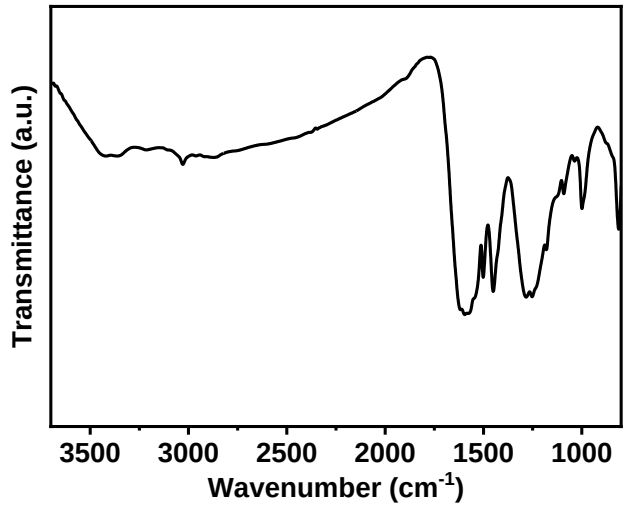

Supplementary Figure 1. FT-IR spectrum of BD-COF.

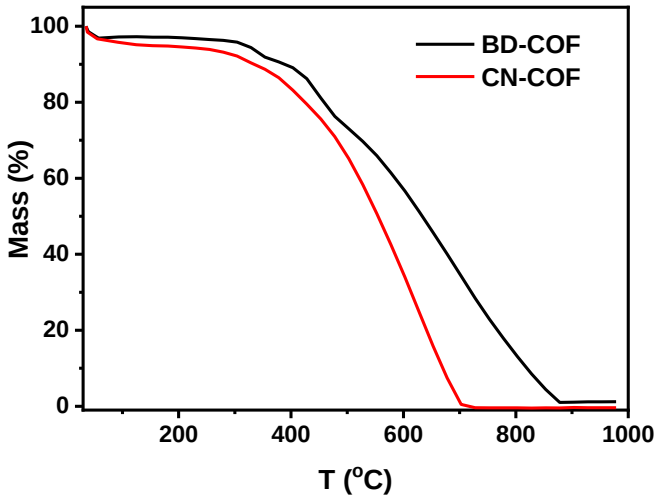

Supplementary Figure 2. TG curves of BD-COF and CN-COF under air atmosphere.

Supplementary Table 1. Fractional atomic coordinated for unit cell of CN-COF (AA stacking) calculated using the Materials Studio modeling program after performing the Pawley Refinement.

Space group		P6/M	
Calculated cell parameters		a = b = 28.781 Å, c = 3.5954 Å, α = β = 90°, γ = 120°, R_p = 3.99%, R_{wp} = 4.91%	
atoms	x	y	z
C1	0.72406	0.36341	0.5
C2	0.6946	0.39125	0.5
O3	0.71734	0.44005	0.5
C4	0.7756	0.38743	0.5
N5	0.81128	0.44314	0.5
C6	0.86599	0.46069	0.5
C7	0.88424	0.42341	0.5
C8	0.93572	0.43926	0.5
C9	0.9725	0.49294	0.5
C10	0.95542	0.53154	0.5
C11	0.90218	0.51541	0.5
C12	0.88604	0.55566	0.5
N13	0.87327	0.58791	0.5
H14	0.79033	0.36108	0.5
H15	0.80037	0.47236	0.5
H16	0.86264	0.38054	0.5
H17	0.94414	0.40698	0.5
H18	0.98086	0.57429	0.5

Supplementary Table 2. Fractional atomic coordinated for unit cell of CN-COF (AB stacking) calculated using the Materials Studio modeling program after performing the Pawley Refinement.

Space group		P63/M	
Calculated cell parameters		a = b = 28.781 Å, c = 7.191 Å, α = β = 90°, γ = 120°	
atoms	x	y	z
C1	1.05739	0.03008	0.25
C2	1.02794	0.05792	0.25
O3	1.05067	0.10672	0.25
C4	1.10893	0.05409	0.25
N5	1.14462	0.10981	0.25
C6	1.19932	0.12735	0.25
C7	1.21757	0.09008	0.25
C8	1.26905	0.10593	0.25
C9	1.30583	0.1596	0.25
C10	1.28876	0.19821	0.25
C11	1.23551	0.18207	0.25
C12	1.21937	0.22232	0.25
N13	1.2066	0.25458	0.25
H14	1.12367	0.02774	0.25
H15	1.1337	0.13902	0.25
H16	1.19597	0.0472	0.25
H17	1.27747	0.07365	0.25
H18	1.3142	0.24095	0.25
C19	0.60928	0.30325	0.25
C20	0.63873	0.27541	0.25
O21	0.616	0.22661	0.25
C22	0.55774	0.27924	0.25
N23	0.52205	0.22353	0.25
C24	0.46735	0.20598	0.25
C25	0.44909	0.24325	0.25

C26	0.39761	0.2274	0.25
C27	0.36083	0.17373	0.25
C28	0.37791	0.13512	0.25
C29	0.43115	0.15126	0.25
C30	0.4473	0.11101	0.25
N31	0.46007	0.07876	0.25
H32	0.543	0.30559	0.25
H33	0.53296	0.19431	0.25
H34	0.47069	0.28613	0.25
H35	0.3892	0.25968	0.25
H36	0.35247	0.09238	0.25

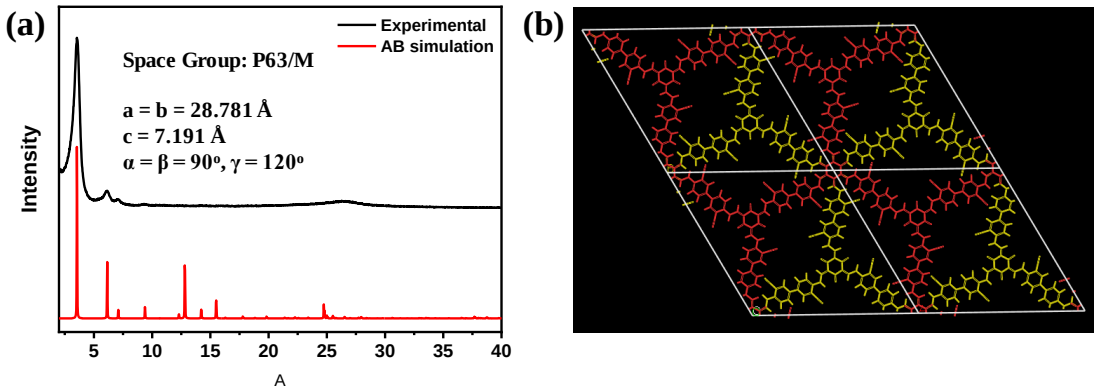

Supplementary Figure 3. (a) Simulated PXRD pattern of staggered models and (b) reproduced AB stacking crystal structure of CN-COF.

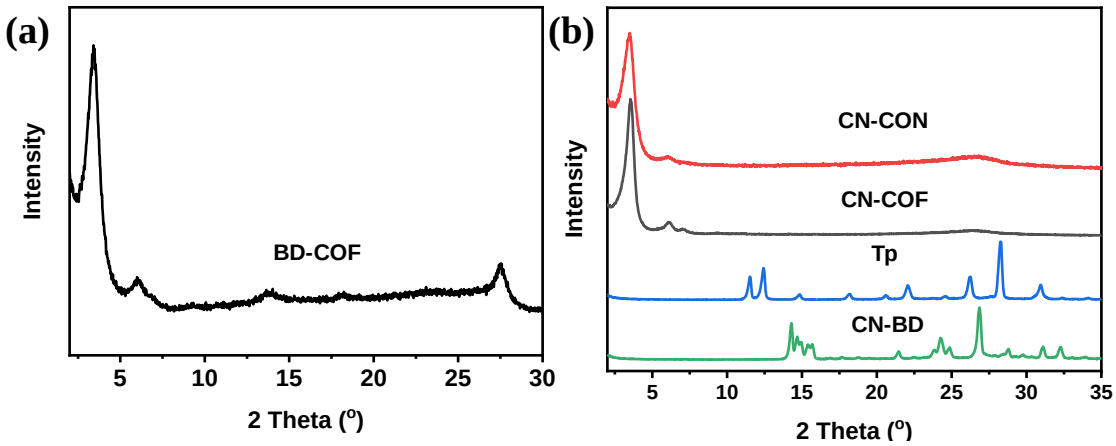

Supplementary Figure 4. PXRD patterns of (a) BD-COF, (b) CN-CON, CN-COF, Tp and CN-BD.

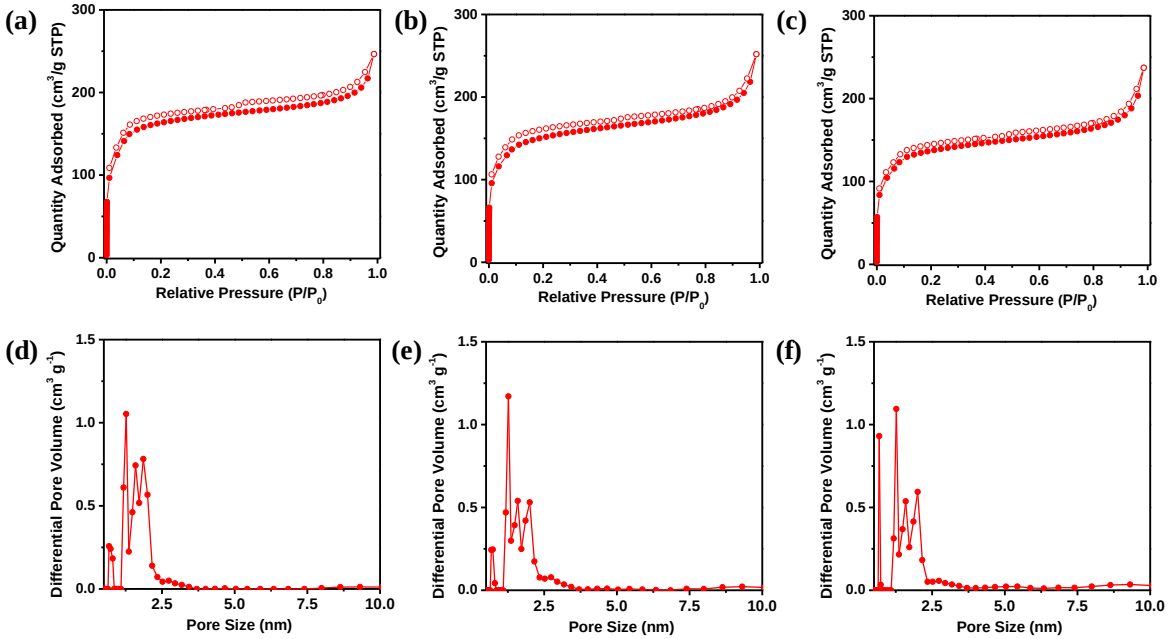

Supplementary Figure 5. (a-c) N_2 adsorption and desorption isotherms and (d-f) pore size distributions calculated by NLDFT of (a,d) CN-COF, (b,e) BD-COF and (c,f) BD-CON.

Supplementary Table 3. The textural parameters of COFs.

Sample	Surface area (m^2 g^{-1})	Pore volume (cm^3 g^{-1})	Pore size (nm)
BD-COF	519	0.39	1.0-2.5
BD-CON	472	0.37	0.7, 1.0-2.5
CN-COF	559	0.60	1.0-2.5
CN-CON	356	0.28	1.0-2.5

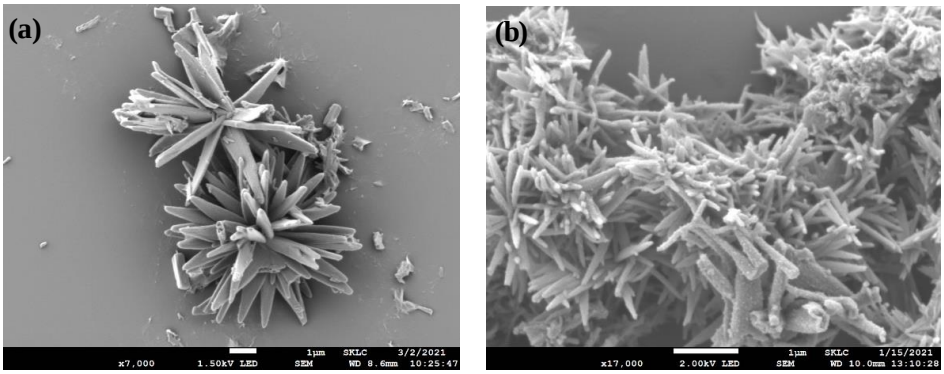

Supplementary Figure 6. SEM images of (a) BD-COF and (b) CN-COF (scale bar: 1 μm).

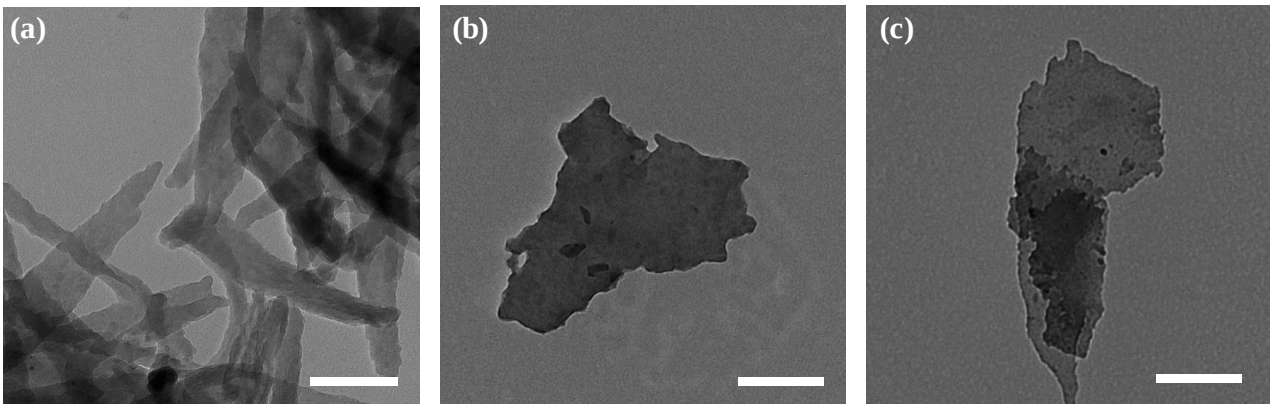

Supplementary Figure 7. TEM images of (a) CN-COF, (b) CN-CON and BD-CON (scale bar: 200 nm).

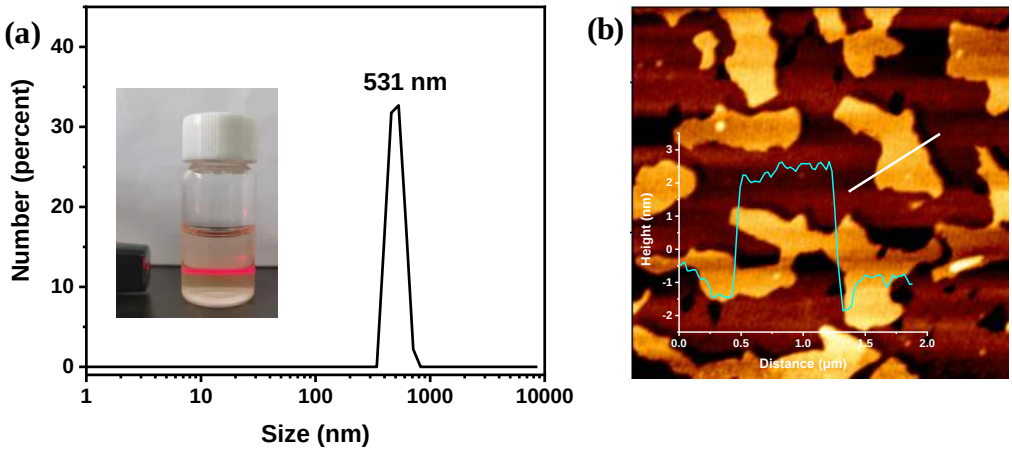

Supplementary Figure 8. (a) Particle size distribution by dynamic light scattering (inset: observed Tyndall effect) and (b) AFM image of BD-CON (inset: height plot).

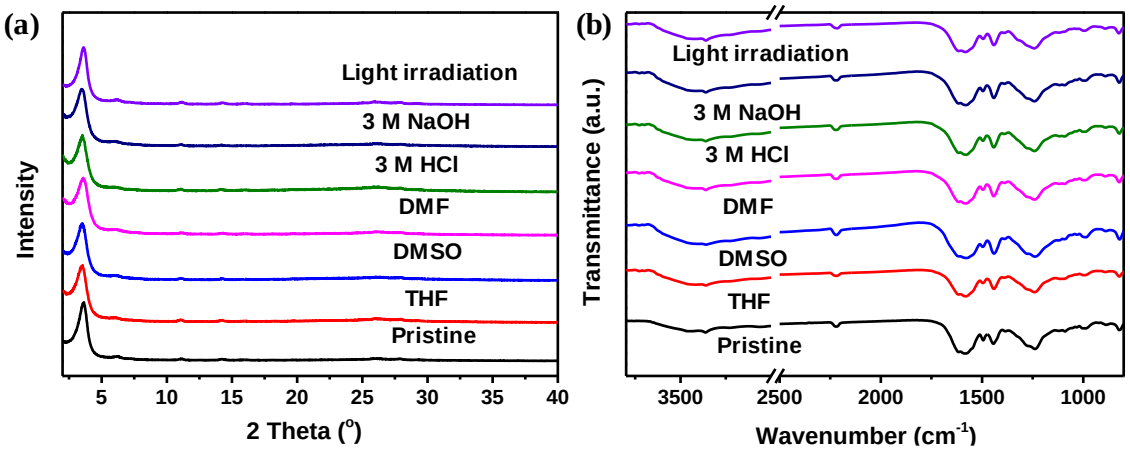

Supplementary Figure 9. (a) PXRD patterns and (b) FT-IR spectra of CN-COF after treatment in 3 M NaOH, 3 M HCl, DMF, DMSO, THF and light irradiation in water for 3 days using a 300 W Xe lamp.

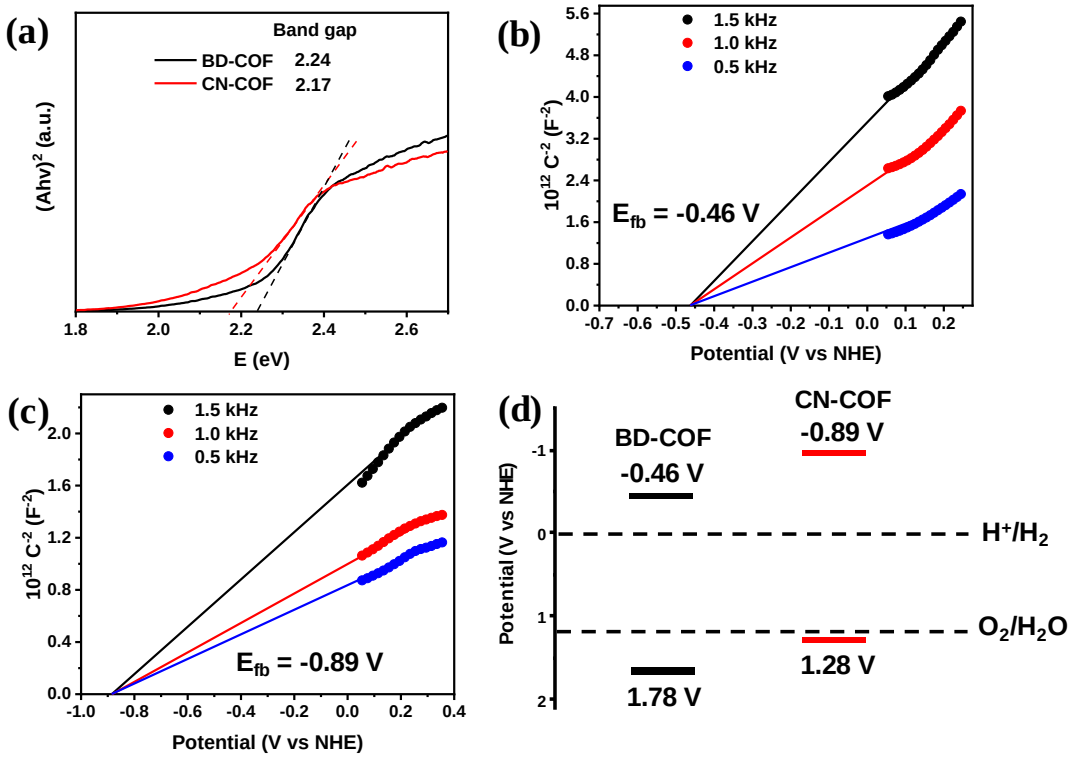

Supplementary Figure 10. (a) Tauc plots of BD-COF and CN-COF. Mott-Schottky plots for (b) BD-COF and (c) CN-COF in 0.2 M Na_2SO_4 aqueous solution with the photocatalyst-coated FTO as work electrode, a platinum foil as the counter electrode, and a saturated calomel electrode as the reference electrode at frequency of 0.5k, 1k and 2k Hz. (d) Schematic energy band structures of BD-COF and CN-COF.

Supplementary Table 4. Hydrogen evolution performance for CN-COF using different scavengers.[a]

Scavenger	Ascorbic acid (0.1 M)	Sodium ascorbate (0.1 M)	Na_2SO_3 (0.1 M)	TEOA (10 vol.%)
HER (μmol h^{-1})	1217	104	8.35	17.2

[a] Reaction conditions: 20 mg of CN-COF was suspended in 100 mL of an aqueous solution of the sacrificial donor (ascorbic acid, sodium ascorbate, Na_2SO_3 or TEOA) with corresponding concentrations, irradiated by a 300 W Xe lamp (λ > 420 nm).

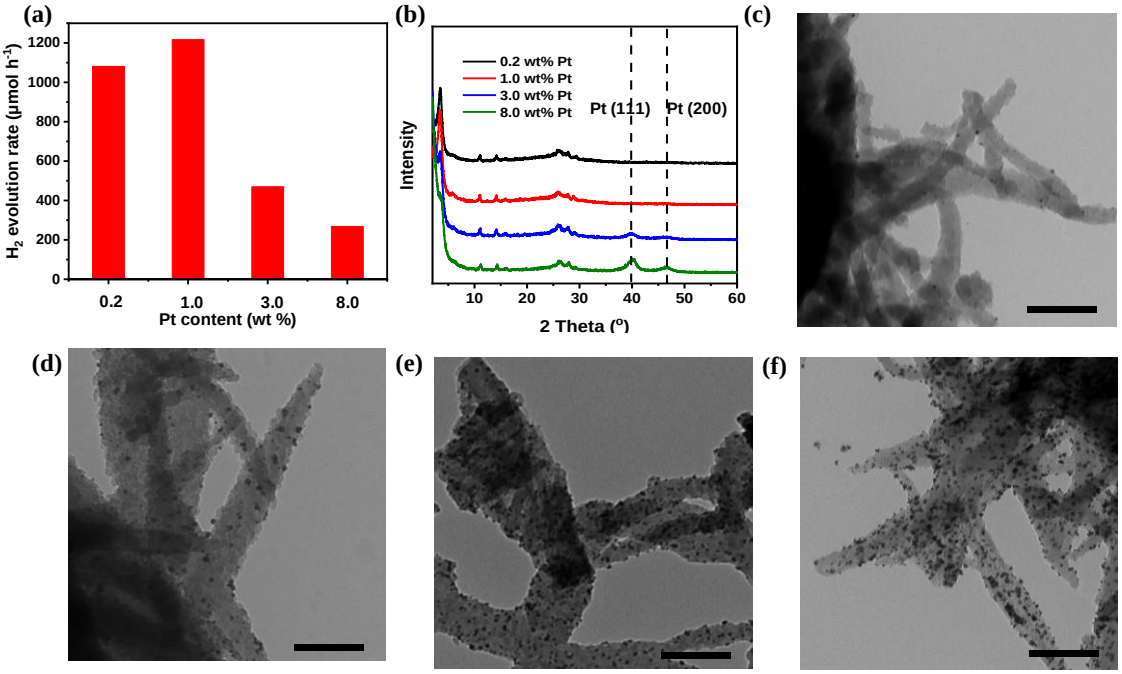

Supplementary Figure 11. (a) Pt content dependent PHE activity of CN-COF, (b) PXRD patterns of CN-COF with different Pt content, TEM images of photo-deposition (c) 0.2 wt% Pt, (d) 1.0 wt% Pt, (e) 3.0 wt% Pt and (f) 8.0 wt% Pt over CN-COF (scale bar: 200 nm).

Supplementary Table 5. Comparison of photocatalytic hydrogen evolution performances of CN-CON with representative COFs and COF-based composites.

Photocatalyst	λ (nm)	Sacrificial reagent	Reaction parameters	Co-cat.	HER (μmol h^{-1})	HER (μmol g^{-1} h^{-1})	AQE %	Ref.
CN-CON	>420	AA	20 mg CON, 0.1 M AA (100 mL)	Pt (1 wt%)	2684	134200	82.6 (at 450 nm)	This work
CN-COF	>420	AA	20 mg COF, 0.1 M AA (100 mL)	Pt (1 wt%)	1217	60850	-	This work
NKCOF-108	>420	AA	10 mg COF, 0.1 M AA (100 mL)	Pt (5 wt%)	120	11600	2.96 (at 520 nm)	[7]
CTF-HUST-A1	>420	TEOA	50 mg COF, 10 mL TEOA, 90 mL H_2O	Pt (3 wt%)	460	9200	7.4 (at 420 nm)	[8]
Py-ClTP-BT-COF	>420	AA	20 mg COF, 0.1 M AA (50 mL)	Pt (5 wt%)	177.5	8875	8.45 (at 420 nm)	[9]
FS-COF+WS5F	>420	AA	5 mg COF, 0.1 M AA (25 mL)	Pt (8 wt%)	81.5	16300	~7.2 (at 420 nm)	[10]
g-$C_{18}N_3$-COF	>420	AA	50 mg COF, 1 M AA (100 mL)	Pt (3 wt%)	14.6	292	1.06 (at 420 nm)	[11]
sp^2c-COF_{ERDN}	>420	TEOA	50 mg COF, 10 mL TEOA, 90 mL H_2O	Pt (3 wt%)	106	2120	0.46 (at 420 nm)	[12]
TpPa-$COF(CH_3)_2$	>420	Sodium ascorbate (SA)	10 mg COF, 50 mL PBS buffer (pH = 7)	Pt (3 wt%)	83.3	8330	-	[13]
CTF-HUST-C1	>420	TEOA	50 mg COF, 10 mL TEOA, 90 mL H_2O	Pt (3 wt%)	255	5100	-	[14]
g-$C_{40}N_3$-COF	>420	TEOA	50 mg COF, 10 mL TEOA, 100 mL H_2O	Pt (3 wt%)	206	4120	4.84 (at 420 nm)	[15]
g-$C_{54}N_6$-COF	>420	TEOA	50 mg COF, 10 mL TEOA,	Pt (3 wt%)	126	2519	-	[16]

ter-CTF-0.7	>420	TEOA	100 mL H_2O 50 mg COF, 10 mL TEOA, 90 mL H_2O	Pt (2 wt%)	966	19300	22.8 (at 420 nm)	[17]
ZnPor-DETH-COF	>400	TEOA	2.5 mg COF, 5 mL PBS buffer (pH = 7), TEOA (50 μL)	Pt (8 wt%)	1.03	413	0.063 (at 450 nm)	[18]
Tp-2C/BPy^{2+}-COF	>420	AA	10 mg COF, 0.1 M AA (100 mL)	Pt (3 wt%)	346	34600	6.93 (at 420 nm)	[19]
TpPa-Cl_2	>420	SA	10 mg COF, 50 mL PBS buffer (pH = 7)	Pt (3 wt%)	76	7600	17.0 (at 400 nm)	[20]
TtaTfa	>420	AA	3 mg COF, 0.1 M AA (16 mL)	Pt (8 wt%)	62.1	20700	1.43 (at 450 nm)	[21]
CdS-CTF-1	>420	Lactic acid (LA)	20 mg photocatalyst, 8 mL LA, 80 mL H_2O	Pt (1 wt%)	228.6	11430	16.3 (at 420 nm)	[22]
TiO_2-TaPa-1-COF	>420	SA	10 mg photocatalyst, 50 mL PBS buffer (pH = 7)	Pt (3 wt%)	111.9	11190	7.6 (at 420 nm)	[23]
g-C_3N_4-COF	>420	TEOA	10 mg photocatalyst, 20 mL TEOA, 180 mL H_2O	Pt (2 wt%)	1005.8	10058	20.7 (at 425 nm)	[24]
MoS_2/TpPa-1-COF	>420	AA	10 mg photocatalyst, 100 mg AA, 50 mL H_2O	-	55.9	5590	0.76 (at 420 nm)	[25]
CdS-COF	>420	LA	30 mg photocatalyst, 1 mL LA, 9 mL H_2O	Pt (0.5 wt%)	110.3	3678	4.2 (at 420 nm)	[26]
Pt-PVP-TP-COF	>420	AA	10 mg photocatalyst, 950 mg AA, 100 mL H_2O	Pt (6 wt%)	84.2	8420	0.4 (at 475 nm)	[27]
CNS-COF	>420	TEOA	20 mg photocatal	Pt (3 wt%)	928	46400	31.8 (at	[28]

			yst, 20 mL TEOA, 180 mL H_2O				425 nm)	
30%PEG@BT-COF	>420	AA	10 mg photocatalyst, 0.1 M AA (100 mL)	Pt (3.5 wt%)	111.4	11140	11.2 (at 420 nm)	[29]
COF-CN	>420	SA	30 mg photocatalyst, 50 mL PBS buffer (pH = 7)	Pt (3 wt%)	384	12800	15.1 (at 500 nm)	[30]
TiO_2/TbBd	>380	TEOA	10 mg photocatalyst, 1 mL TEOA, 9 mL H_2O	Pt (3 wt%)	39.6	3962	-	[31]

Supplementary Table 6. Comparison of photocatalytic hydrogen evolution performances of CN-CON with representative polymer and polymer-based composites.

Photocatalyst	λ (nm)	Sacrificial reagent	Reaction parameters	Co-cat.	HER (μmol h^{-1})	HER (μmol g^{-1} h^{-1})	AQE %	Ref.
CN-CON	>420	AA	20 mg CON, 0.1 M AA (100 mL)	Pt (1 wt%)	2684	134200	82.6 (at 450 nm)	This work
CN-COF	>420	AA	20 mg COF, 0.1 M AA (100 mL)	Pt (1 wt%)	1217	60850	-	This work
PyBS-3	>420	AA	10 mg photocatalyst, 10 mL DMF, 1 M AA (90 mL)	Pt (3 wt%)	430	43000	29.3 (at 420 nm)	[32]
PyBS-3	>300	AA	10 mg photocatalyst, 10 mL DMF, 1 M AA (90 mL)	Pt (3 wt%)	1050	105000	-	[32]
S-CMP-3	>420	TEA	25 mg photocatalyst, H_2O : TEA :MeOH (1:1:1 vol, 25 mL)	Pd (0.7 wt%)	77.7	3106	13.2 (at 420 nm)	[33]
P10	>420	TEA	25 mg photocatalyst, H_2O : TEA :MeOH (1:1:1 vol, 25 mL)	Pd (0.4 wt%)	81.5	3260	11.6 (at 420 nm)	[34]
PDBTSO	>420	TEOA	10 mg photocatalys	Pt (3 wt%)	442	44200	-	[35]

TxPP1@T-10	Uv-vis	MeOH	t, 20 mL TEOA, 80 mL H_2O, 2 mmol K_2HPO_4 100 mg photocatalyst, 100 mL MeOH, 900 mL H_2O	Pt (1 wt%)	2194.5	21945	-	[36]
P10-e	>420	MeOH/TEA	2.5 mg photocatalyst, H_2O : TEA :MeOH (1:1:1 vol, 25 mL)	Pd (0.4 wt%)	36.3	14520	20.4 (at 420 nm)	[37]
TiO_2@BpZn-COP	>420	TEOA	20 mg photocatalyst, 15 mL TEOA, 85 mL H_2O	Pt (3 wt%)	26.6	1333	2.5 (at 420 nm)	[38]
PDBTSO@TiO_2	>420	TEOA	10 mg photocatalyst, 20 mL TEOA, 80 mL H_2O	Pt (3 wt%)	515	51500	13 (at 420 nm)	[39]
P3HT-g-C_3N_4	>500	AA	10 mg photocatalyst, 1 M AA (10 mL)	Pt (1 wt%)	3045	304500	77.4 (at 420 nm)	[40]
Co-S/g-C_3N_4	AM1.5G	TEOA	5 mg photocatalyst, 6 mL TEOA, 44 mL H_2O	-	51.6	10329	-	[41]
α-Fe_2O_3/g-C_3N_4	>400	TEOA	10 mg photocatalyst, 10 mL TEOA, 90 mL H_2O	Pt (3 wt%)	314	31400	44.4 (at 420 nm)	[42]
CN-L0.10	>420	TEOA	10 mg photocatalyst, 5 mL TEOA, 45 mL H_2O	Pt (3 wt%)	22.3	2235	4.8 (at 420 nm)	[43]
g-C_3N_4 nanomesh	>420	TEOA	10 mg photocatalyst, 10 mL TEOA, 90 mL H_2O	Pt (3 wt%)	85.1	8510	5.1 (at 420 nm)	[44]
GD-C_3N_4	>420	TEOA	10 mg photocatalyst, 10 mL TEOA, 100 mL H_2O	Pt (3 wt%)	230.6	23060	31.1 (at 420 nm)	[45]

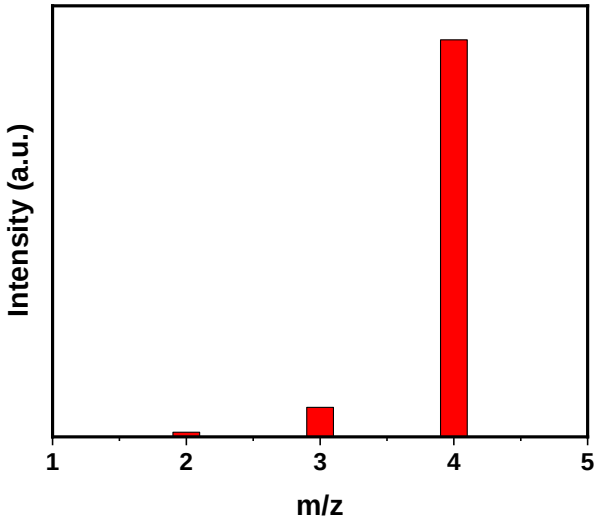

Supplementary Figure 12. Isotope labeling experiment was conducted by using D_2O instead of H_2O for photocatalytic hydrogen evolution which exhibits the evolution of D_2 gas.

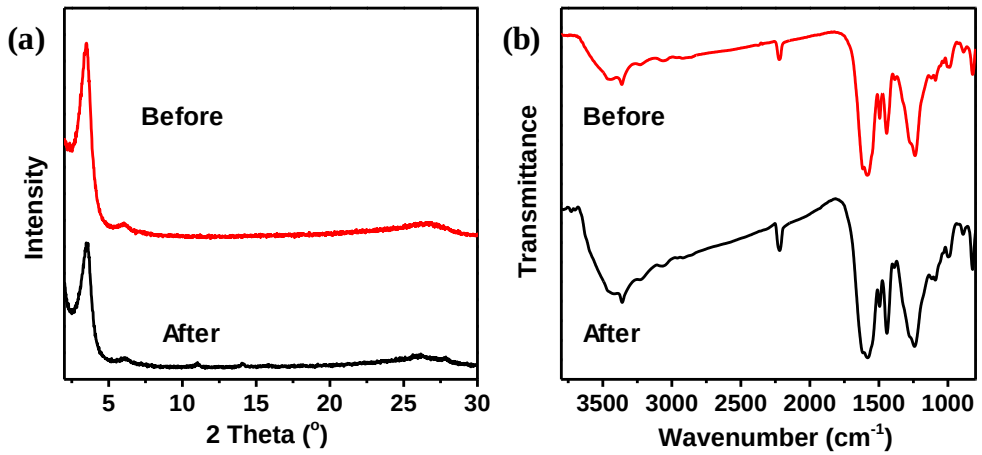

Supplementary Figure 13. (a) PXRD pattern and (b) FT-IR spectrum of CN-CON before and after several catalytic cycles.

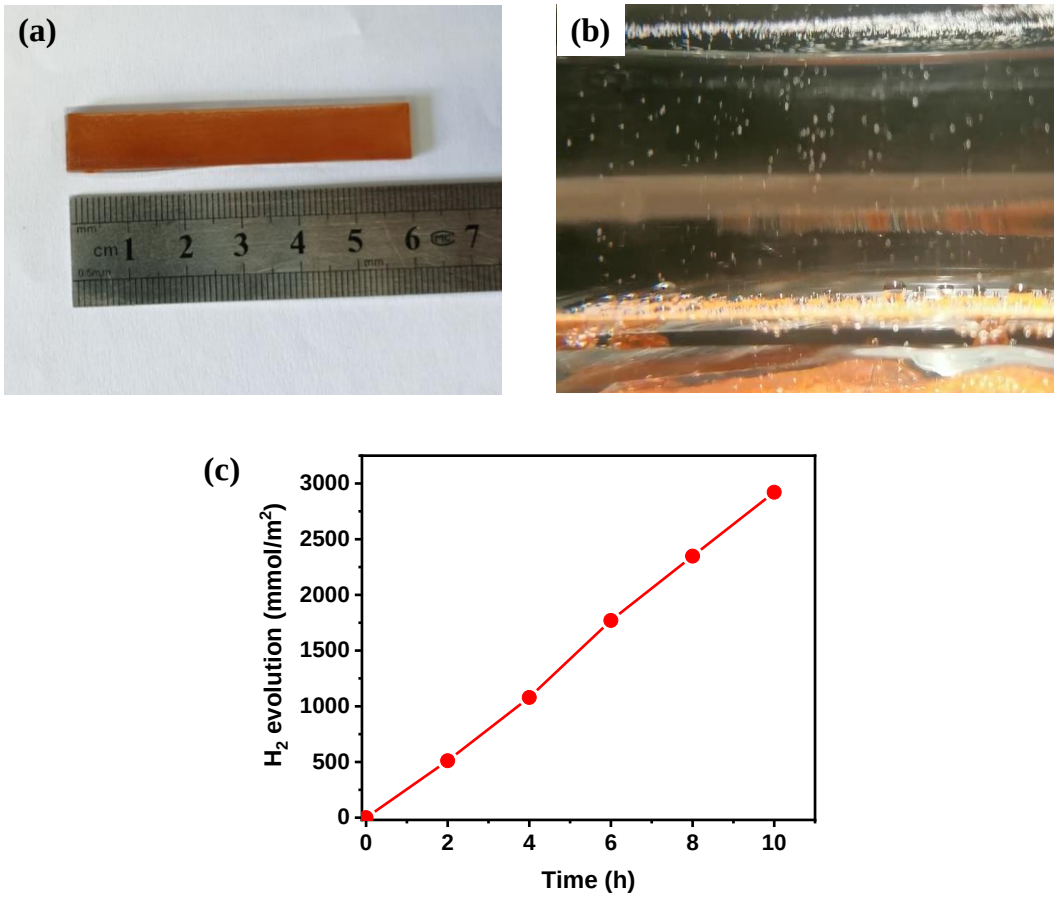

Supplementary Figure 14. (a) Photograph of as-prepared CN-CON film on glass, (b) photograph showing hydrogen evolution with CN-CON film on glass, (c) time course of photocatalytic H_2 evolution for CN-CON film on glass.

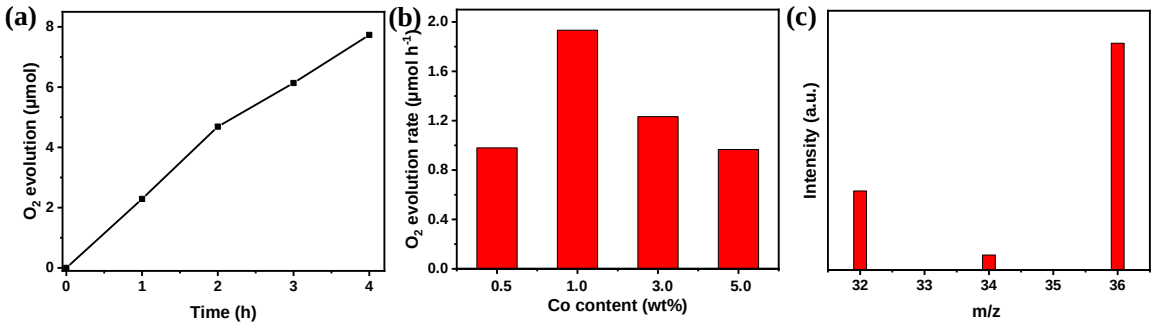

Supplementary Figure 15. (a) Time course of photocatalytic O_2 production for CN-CON (20 mg catalyst in 100 mL water, 100 mg La_2O_3, 5 mmol $AgNO_3$, $\lambda > 420$ nm). (b) Co content dependent oxygen evolution activity of CN-CON. (c) Isotope labeling experiment was conducted by using $H_2{}^{18}O$ instead of H_2O for photocatalytic oxygen evolution which exhibits the evolution of $^{18}O_2$ gas.

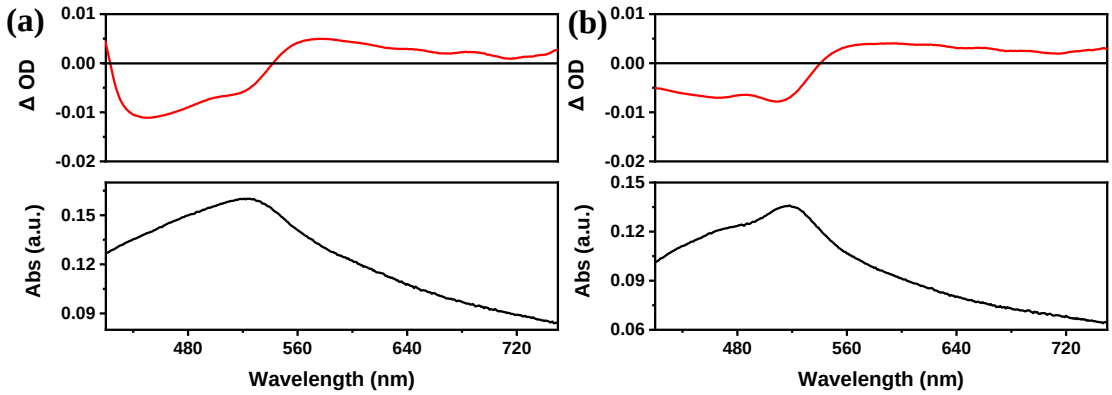

Supplementary Figure 16. TA spectra (red line) at 2 ps and steady-state absorption spectra (black line) of (a) BD-CON and (b) CN-CON.

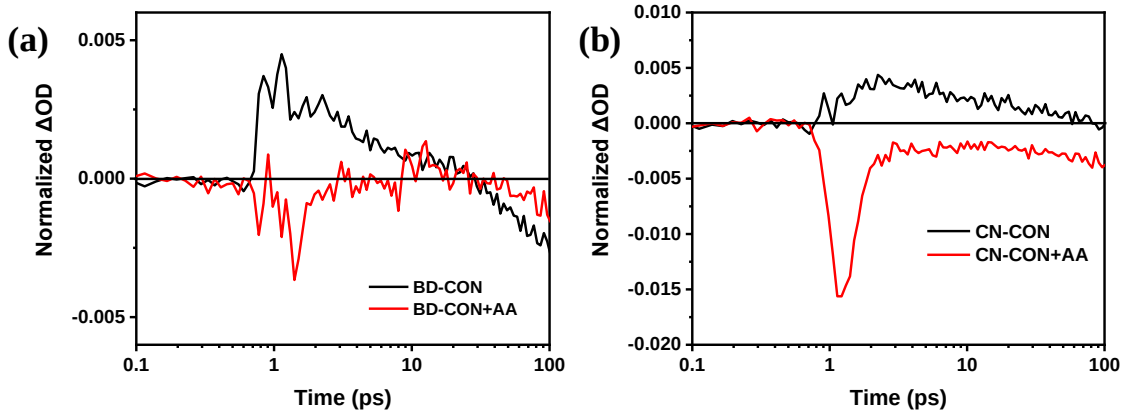

Supplementary Figure 17. TA kinetics of (a) BD-CON and (b) CN-CON probed at 650 nm (trapped hole). In the presence of 0.1 M AA, the hole signal disappeared with the appearance of a negative absorption peak assigned to an ultra-fast component stemming from hole transfer from VB of CONs to the hole scavenger.

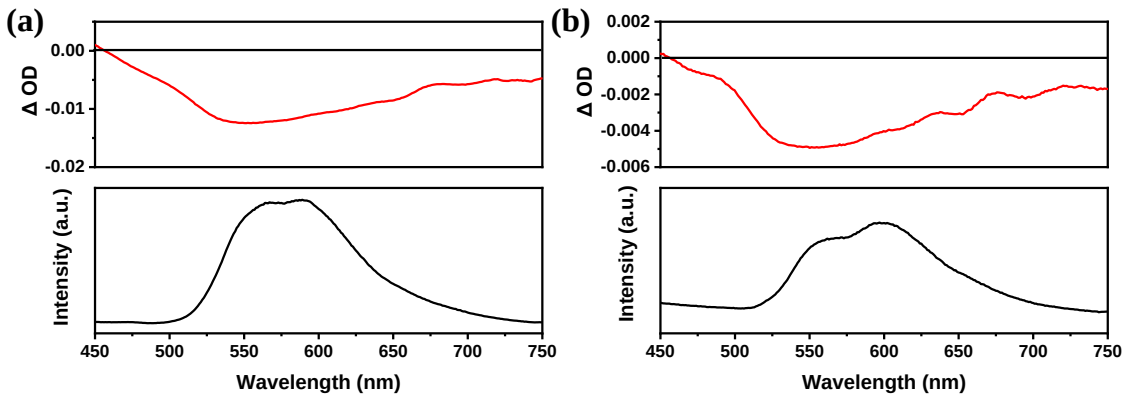

Supplementary Figure 18. TA spectra (red line) at 1 ns and steady-state PL spectra (black line) with excitation wavelength at 380 nm of (a) BD-CON and (b) CN-CON.

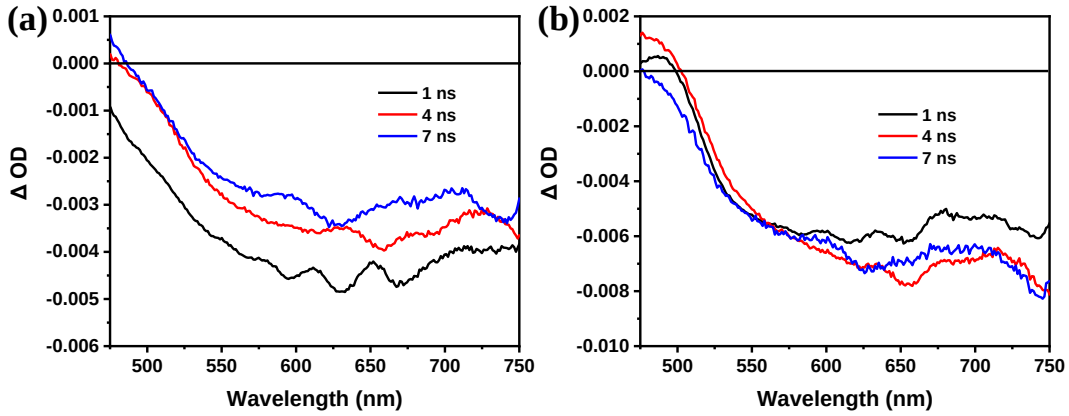

Supplementary Figure 19. Time slices of the TA spectra of CN-CON in 0.1 M ascorbic acid of (a) BD-CON and (b) CN-CON. The negative signals can be attributed to long-lived electron in the presence of 0.1 M ascorbic acid.

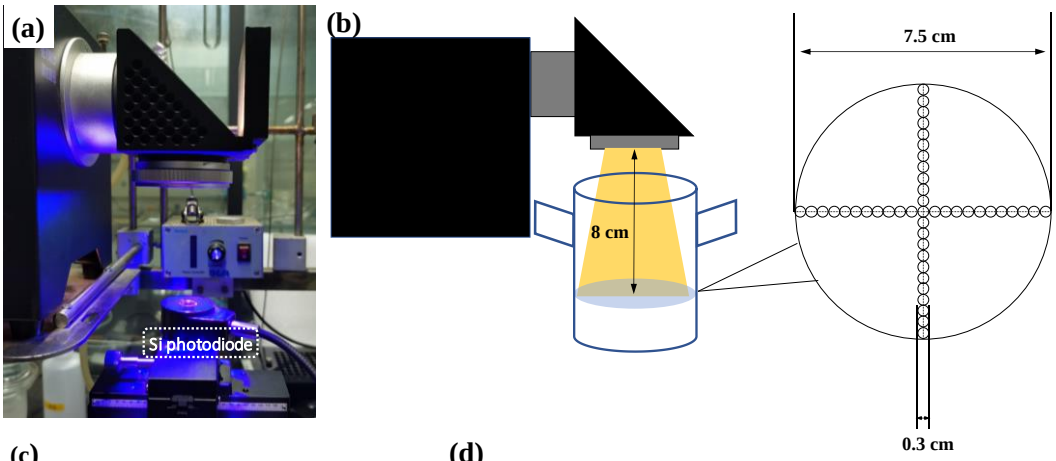

(d)

Wavelength (nm)	Number of incident photons per hour	H_2 evolution (μmol h^{-1})	AQE (%)
400	4.14×10^{20}	279.54	81.3
450	7.71×10^{20}	528.97	82.6
500	9.58×10^{20}	644.49	81.0
550	1.37×10^{21}	588.37	51.7
600	1.33×10^{21}	194.67	17.6
650	1.16×10^{21}	39.98	4.2

Supplementary Figure 20. (a) Photographs of the devices used in the AQE measurement, (b) illustration of photon-counting system, (c) the relation of photon numbers and wavelength using different band-pass filters (measured at the center of light spot, diameter of 3 mm), (d) summary of the number of incident photons, PHE activity and AQE at different wavelengths.

Supplementary references.

[1] G. Kresse, J. Furthmüller, *Comput. Mater. Sci.* **1996**, *6*, 15-50.

[2] G. Kresse, J. Furthmüller, *Phys. Rev. B* **1996**, *54*, 11169-11186.

[3] J. P. Perdew, K. Burke, M. Ernzerhof, *Phys. Rev. Lett.* **1996**, *77*, 3865-3868.

[4] G. Kresse, D. Joubert, *Phys. Rev. B* **1999**, *59*, 1758-1775.

[5] H. J. Monkhorst, J. D. Pack, *Phys. Rev. B*, **1976**, *13*, 5188-5192.

[6] T. Takata, J. Jiang, Y. Sakata, M. Nakabayashi, N. Shibata, V. Nandal, K. Seki, T. Hisatomi, K. Domen, *Nature* **2020**, *581*, 411-414.

[7] Z. Zhao, Y. Zheng, C. Wang, S. Zhang, J. Song, Y. Li, S. Ma, P. Cheng, Z. Zhang, Y. Chen, *ACS Catal.* **2021**, *11*, 2098-2107.

[8] S. Zhang, G. Cheng, L. Guo, N. Wang, B. Tan, S. Jin, *Angew. Chem. Int. Ed.* **2020**, *59*, 6007-6014.

[9] W. Chen, L. Wang, D. Mo, F. He, Z. Wen, X. Wu, H. Xu, L. Chen, *Angew. Chem. Int. Ed.* **2020**, *59*, 16902-16909.

[10] X. Wang, L. Chen, S. Y. Chong, M. A. Little, Y. Wu, W.-H. Zhu, R. Clowes, Y. Yan, M. A. Zwijnenburg, R. S. Sprick, A. I. Cooper, *Nat. Chem.* **2018**, *10*, 1180-1189.

[11] S. Wei, F. Zhang, W. Zhang, P. Qiang, K. Yu, X. Fu, D. Wu, S. Bi, F. Zhang, *J. Am. Chem. Soc.* **2019**, *141*, 14272-14279.

[12] E. Jin, Z. Lan, Q. Jiang, K. Geng, G. Li, X. Wang, D. Jiang, *Chem* **2019**, *5*, 1632-1647.

[13] J.-L. Sheng, H. Dong, X.-B. Meng, H.-L. Tang, Y.-H. Yao, D.-Q. Liu, L.-L. Bai, F.-M. Zhang, J.-Z. Wei, X.-J. Sun, *ChemCatChem* **2019**, *11*, 2313-2319.

[14] M. Liu, Q. Huang, S. Wang, Z. Li, B. Li, S. Jin, B. Tan, *Angew. Chem. Int. Ed.* **2018**, *57*, 11968-11972.

[15] S. Bi, C. Yang, W. Zhang, J. Xu, L. Liu, D. Wu, X. Wang, Y. Han, Q. Liang, F. Zhang, *Nat. Commun.* **2019**, *10*, 2467.

[16] J. Xu, C. Yang, S. Bi, W. Wang, Y. He, D. Wu, Q. Liang, X. Wang, F. Zhang, *Angew. Chem. Int. Ed.* **2020**, *59*, 23845-23853.

[17] L. Guo, Y. Niu, S. Razzaque, B. Tan, S. Jin, *ACS Catal.* **2019**, *9*, 9438-9445.

[18] R. Chen, Y. Wang, Y. Ma, A. Mal, X.-Y. Gao, L. Gao, L. Qiao, X.-B. Li, L.-Z. Wu, C. Wang, *Nat. Commun.* **2021**, *12*, 1354.

[19] Z. Mi, T. Zhou, W. Weng, J. Unruangsri, K. Hu, W. Yang, C. Wang, K. A. I.

Zhang, J. Guo, *Angew. Chem. Int. Ed.* **2021**, *60*, 9642-9649.

[20] L. Yin, Y. Zhao, Y. Xing, H. Tan, Z. Lang, W. Ho, Y. Wang, Y. Li, *Chem. Eng. J.* **2021**, *419*, 129984.

[21] J. Yang, A. Acharjya, M.-Y. Ye, J. Rabeah, S. Li, Z. Kochovski, S. Youk, J. Roeser, J. Grüneberg, C. Penschke, M. Schwarze, T. Wang, Y. Lu, R. van de Krol, M. Oschatz, R. Schomäcker, P. Saalfrank, A. Thomas, *Angew. Chem. Int. Ed.* **2021**, *60*, 19797-19803.

[22] D. Wang, H. Zeng, X. Xiong, M.-F. Wu, M. Xia, M. Xie, J.-P. Zou, S.-L. Luo, *Sci. Bull.* **2020**, *65*, 113-122.

[23] C.-C. Li, M.-Y. Gao, X.-J. Sun, H.-L. Tang, H. Dong, F.-M. Zhang, *Appl. Catal. B* **2020**, *266*, 118586.

[24] M. Luo, Q. Yang, K. Liu, H. Cao, H. Yan, *Chem. Commun.* **2019**, *55*, 5829-5832.

[25] M.-Y. Gao, C.-C. Li, H.-L. Tang, X.-J. Sun, H. Dong, F.-M. Zhang, *J. Mater. Chem. A* **2019**, *7*, 20193-20200.

[26] J. Thote, H. B. Aiyappa, A. Deshpande, D. D. Díaz, S. Kurungot, R. Banerjee, *Chem. Eur. J.* **2014**, *20*, 15961-15965.

[27] J. Ming, A. Liu, J. Zhao, P. Zhang, H. Huang, H. Lin, Z. Xu, X. Zhang, X. Wang, J. Hofkens, M. B. J. Roeffaers, J. Long, *Angew. Chem. Int. Ed.* **2019**, *58*, 18290-18294.

[28] M. Luo, Q. Yang, W. Yang, J. Wang, F. He, K. Liu, H. Cao, H. Yan, *Small* **2020**, *16*, 2001100.

[29] T. Zhou, L. Wang, X. Huang, J. Unruangsri, H. Zhang, R. Wang, Q. Song, Q. Yang, W. Li, C. Wang, K. Takahashi, H. Xu, J. Guo, *Nat. Commun.* **2021**, *12*, 3934.

[30] Y. Xing, L. Yin, Y. Zhao, Z. Du, H.-Q. Tan, X. Qin, W. Ho, T. Qiu, Y.-G. Li, *ACS Appl. Mater. Interfaces* **2020**, *12*, 51555-51562.

[31] L. Liu, J. Zhang, X. Tan, B. Zhang, J. Shi, X. Cheng, D. Tan, B. Han, L. Zheng, F. Zhang, *Nano Res.* **2020**, *13*, 983-988.

[32] C. Shu, C. Han, X. Yang, C. Zhang, Y. Chen, S. Ren, F. Wang, F. Huang, J.-X. Jiang, *Adv. Mater.* **2021**, *33*, 2008498.

[33] R. S. Sprick, Y. Bai, A. A. Y. Guilbert, M. Zbiri, C. M. Aitchison, L. Wilbraham, Y. Yan, D. J. Woods, M. A. Zwijnenburg, A. I. Cooper, *Chem. Mater.* **2019**, *31*, 305-313.

[34] M. Sachs, R. S. Sprick, D. Pearce, S. A. J. Hillman, A. Monti, A. A. Y. Guilbert,

N. J. Brownbill, S. Dimitrov, X. Shi, F. Blanc, M. A. Zwijnenburg, J. Nelson, J. R. Durrant, A. I. Cooper, *Nat. Commun.* **2018**, *9*, 4968.

[35] G. Shu, Y. Li, Z. Wang, J.-X. Jiang, F. Wang, *Appl. Catal. B* **2020**, *261*, 118230.

[36] A. Valverde-González, C. G. L. Calixto, M. Barawi, M. Gomez-Mendoza, V. A. de la P. O'Shea, M. Liras**,** B. Gómez-Lor**,** M. Iglesias**,** *ACS Appl. Energy Mater.* **2020**, *3*, 4411-4420.

[37] C. M. Aitchison, R. S. Sprick, A. I. Cooper, *J. Mater. Chem. A* **2019**, *7*, 2490-2496.

[38] J. Chen, X. Tao, L. Tao, H. Li, C. Li, X. Wang, C. Li, R. Li, Q. Yang, *Appl. Catal. B* **2019**, *241*, 461-470.

[39] G. Shu, Y. Wang, Y. Li, S. Zhang, J.-X. Jiang, F. Wang, *J. Mater. Chem. A* **2020**, *8*, 18292-18301.

[40] X. Zhang, B. Peng, S. Zhang, T. Peng, *ACS Sustainable Chem. Eng.* **2015**, *3*, 1501-1509.

[41] L. Chen, Y. Xu, Z. Yang, K. Zhang, B. Chen, *Appl. Catal. B* **2020**, *277*, 119207.

[42] X. She, J. Wu, H. Xu, J. Zhong, Y. Wang, Y. Song, K. Nie, Y. Liu, Y. Yang, M.-T. F. Rodrigues, R. Vajtai, J. Lou, D. Du, H. Li, P. M. Ajayan, *Adv. Energy Mater.* **2017**, *7*, 1700025.

[43] C. Zhao, C. Ding, C. Han, X. Yang, J. Xu, *Sol. RRL* **2021**, *5*, 2000486.

[44] Q. Han, B. Wang, J. Gao, Z. Cheng, Y. Zhao, Z. Zhang, L. Qu, *ACS Nano* **2016**, *10*, 2745-2751.

[45] Y. Yu, W. Yan, X. Wang, P. Li, W. Gao, H. Zou, S. Wu, K. Ding, *Adv. Mater.* **2018**, *30*, 1705060.